bioRxiv preprint doi: https://doi.org/10.1101/023333; this version posted July 27, 2015. The copyright holder for this preprint (which was not certified by peer review) is the author/funder, who has granted bioRxiv a license to display the preprint in perpetuity. It is made available under aCC-BY-NC 4.0 International license.

Dis-integrating the fly: A mutational perspective on phenotypic integration and covariation.

Running title: Mutational effects on environmental covariation

Authors: Annat Haber[1,2] & Ian Dworkin[1,3,4]

Author affiliations:

1) BEACON Center for the study of Evolution in Action. Michigan State University.

2) Department of Zoology, Tel Aviv University

3) Department of Integrative Biology, Michigan State University.

4) Department of Biology, McMaster University.

Correspondence: annat22@gmail.com, dworkin@mcmaster.ca

Key words: Drosophila, integration, canalization, morphometrics, covariation, mutation

Number of words: 5230

Number of tables: 3

Number of figures: 7

Data will be archived in DRYAD

bioRxiv preprint doi: https://doi.org/10.1101/023333; this version posted July 27, 2015. The copyright holder for this preprint (which was not certified by peer review) is the author/funder, who has granted bioRxiv a license to display the preprint in perpetuity. It is made available under aCC-BY-NC 4.0 International license.

Abstract

The structure of environmentally induced phenotypic covariation can influence the effective strength and magnitude of natural selection. Yet our understanding of the factors that contribute to and influence the evolutionary lability of such covariation is poor. Most studies have examined either environmental variation, without accounting for covariation, or examined phenotypic and genetic covariation, without distinguishing the environmental component. In this study we examined the effect of mutational perturbations on different properties of environmental covariation, as well as mean shape. We use strains of *Drosophila melanogaster* bearing well-characterized mutations known to influence wing shape, as well as naturally-derived strains, all reared under carefully-controlled conditions and with the same genetic background. We find that mean shape changes more freely than the covariance structure, and that different properties of the covariance matrix change independently from each other. The perturbations affect matrix orientation more than they affect matrix size or eccentricity. Yet, mutational effects on matrix orientation do not cluster according to the developmental pathway that they target. These results suggest that it might be useful to consider a more general concept of 'decanalization', involving all aspects of variation and covariation.

bioRxiv preprint doi: https://doi.org/10.1101/023333; this version posted July 27, 2015. The copyright holder for this preprint (which was not certified by peer review) is the author/funder, who has granted bioRxiv a license to display the preprint in perpetuity. It is made available under aCC-BY-NC 4.0 International license.

Introduction

The evolutionary response to natural selection requires phenotypic variation. As such, the mechanisms generating phenotypic variation and covariation (**P**) are of fundamental importance. Most studies focus on the genetic component in **P**, summarized as the genetic covariance matrix **G**, due to its role in the response to natural selection as summarized in the multivariate version of the breeder's equation (Lande 1979; Lande and Arnold 1983). Thus, the generation of heritable components of variation, governed by mutation and recombination, is broadly studied. However non-heritable sources of phenotypic variation, often summarized through **E**, remain important for our understanding of both the magnitude and direction of response to natural selection through its contributions to **P**. The basic measure of the strength of selection - the selection differential - depends on the phenotypic variance of a trait via the covariance of the phenotype and fitness (the Robertson-Price identity; Robertson 1966; Price 1970). More generally, the magnitude of the selection differential is a function of both the shape of the underlying fitness profile (W(z)) and the current population mean and variance for the trait (V_Z) associated with fitness. In addition to its influence on the magnitude of selection, **E** (via **P**) influences the response to selection as summarized in Lande's (1979) equation. When considering a multivariate set of phenotypes, the influence of covariation in **E** becomes increasingly relevant, influencing the orientation of the response to selection. Although environmental covariation may not facilitate adaptive evolution, it can certainly impede it, and possibly bias its trajectory towards a secondary peak (Burger 1986). Yet, our understanding of

bioRxiv preprint doi: https://doi.org/10.1101/023333; this version posted July 27, 2015. The copyright holder for this preprint (which was not certified by peer review) is the author/funder, who has granted bioRxiv a license to display the preprint in perpetuity. It is made available under aCC-BY-NC 4.0 International license.

how this environmental covariation is generated during development is incomplete, as is our understanding of how it evolves.

Mutational and environmental perturbations have often been used to examine how the environmental component of phenotypic variation changes, particularly in the context of canalization (Waddington 1952; Dworkin 2005a,b; Levy and Siegal 2008; Hallgrímsson et al. 2009; Paaby and Rockman 2014; and references therein). Numerous studies have found an increase in phenotypic variance in response to perturbations, often attributed to decanalization, and due in part to a release of cryptic genetic variation. However, both increases and decreases of environmental variance have also been observed without the release of genetic variation. Most studies (e.g., Dworkin 2005a; Levy and Siegal 2008), however, have examined the effect of mutational perturbations on the variance of a trait, or the total variance across several traits, whereas in multivariate systems other aspects of covariation need to be considered.

Covariance matrices have a number of important properties, namely matrix size, shape (eccentricity), and orientation (Jones et al. 2003; Hohenlohe and Arnold 2008), as illustrated in Figure 1. The size of a matrix is measured as the total variance (sum of the individual trait variances) and quantifies variation overall, irrespective of how it is distributed among different directions (Fig. 1A). The orientation of the matrix refers to the direction in which the primary axes of covariation are pointing (Fig. 1B), and is determined by the relative contribution of each trait to each eigenvector. Thus, a change in matrix orientation reflects a change in the direction in which most of the variation is concentrated. The eccentricity of the matrix describes its shape – how much it deviates from a hypersphere – and it quantifies how evenly the variance is distributed among the different directions (Fig. 1C), irrespective of the orientation, and,

bioRxiv preprint doi: https://doi.org/10.1101/023333; this version posted July 27, 2015. The copyright holder for this preprint (which was not certified by peer review) is the author/funder, who has granted bioRxiv a license to display the preprint in perpetuity. It is made available under aCC-BY-NC 4.0 International license.

76 depending on how it is measured, irrespective of matrix size. A more eccentric matrix (i.e. more
77 cigar-shaped) means that there is considerably more variation along the first axis relative to
78 other axes.

79 Previous studies provide mixed expectations as to how the different properties of the
80 covariance matrix would change relative to each other and relative to mean shape. Hallgrímsson
81 et al. (2009) postulated that when the variance increases due to perturbations, matrix
82 eccentricity can either increase or decrease, depending on how the perturbed developmental
83 process contributes to the original patterns of covariation. Eccentricity would increase with total
84 variance if the targeted pathway plays a major role in integrating the measured traits, thus
85 adding variance to the major axis of covariation. When the perturbed pathway does not
86 contribute much to the major axis of covariation, changes in variance are distributed among the
87 smaller subsequent eigenvalues, thus reducing eccentricity.

88 The association between changes to matrix orientation and eccentricity has mostly been
89 studied so far for **P** and **G** rather than **E**, making expectations for **E** far less clear. Simulations by
90 Jones et al. (2003, 2004, 2007, 2012) and Revell (2007) suggest that the orientation of **G** is more
91 likely to change than eccentricity under most conditions, including effects due to population size,
92 magnitude, and orientation of mutational correlation and stabilizing selection, and different
93 modes of directional selection. In addition, higher eccentricity enhances the stability of the
94 orientation under most conditions. The magnitude and stability of eccentricity and matrix size, on
95 the other hand, are mostly influenced by population size rather than mutational correlations and
96 selection. Empirical studies have found evidence that both eccentricity and orientation can be
97 either stable or labile across populations and species at different phylogenetic scales (Arnold et

bioRxiv preprint doi: https://doi.org/10.1101/023333; this version posted July 27, 2015. The copyright holder for this preprint (which was not certified by peer review) is the author/funder, who has granted bioRxiv a license to display the preprint in perpetuity. It is made available under aCC-BY-NC 4.0 International license.

al. 2008; de Oliveira et al. 2009; Porto et al. 2009; Haber 2015a,b). Unfortunately it is not clear whether the expectations from these studies (examining **G** and **P**) are relevant to how **E** changes. Changes in **G** reflect a combination of influences from mutation and other evolutionary forces. The structure of **E**, on the other hand, reflects the interaction between the environment and development. Thus, while strong directional selection can deplete genetic covariation, altering matrix eccentricity and size of **G**, it is not clear *a priori* that this should alter the matrix properties of **E** as well.

Empirical studies have found mutational effects on matrix orientation of **E** that could not be readily associated with developmental pathways or mutational effect size (Hallgrímsson et al. 2006; Debat et al. 2009; Jamniczky and Hallgrímsson 2009). In addition, studies have found both increases and decreases of eccentricity (Hallgrímsson et al. 2009). Most studies, however, did not include a direct comparison of the different properties of **E** and shape variation across a wide range of mutations. Thus, we are left with little understanding of the lability of **E**.

Drosophila wing shape is an ideal system to address these questions, and in particular how mutational perturbations influence the different aspects of the covariance structure of **E**. The development of the wing of *D. melanogaster* has been a model system for over 70 years, and it is one of the best genetically characterized model systems. The extensive set of genetic tools, mutant lines, and ability to generate many genetically identical individuals reared under common environments enables the study of mutational effects on **E**. Variation in both size and shape of the *Drosophila* wing has a long history of research, and sophisticated high dimensional representations of shape can be generated in a high throughput manner (Houle et al. 2003; Pitchers et al. 2013). Studies of de-canalization for *Drosophila* wing shape, and the influence of

bioRxiv preprint doi: https://doi.org/10.1101/023333; this version posted July 27, 2015. The copyright holder for this preprint (which was not certified by peer review) is the author/funder, who has granted bioRxiv a license to display the preprint in perpetuity. It is made available under aCC-BY-NC 4.0 International license.

mutations on aspects of **E** have had mixed results. While mutant perturbation can have profound effects on mean shape (Weber 2005, Breuker et al. 2006; Debat et al. 2006; Dworkin and Gibson 2006; Debat et al. 2009, Debat et al. 2011), the influence on variance has been more mixed, with some studies seeing a general increase (Debat et al. 2009, Debat et al. 2011) and others seeing both increase and decrease (Debat et al. 2006; Dworkin and Gibson 2006). Some evidence for the effect of mutational and environmental perturbations on matrix orientation has been shown in these studies, but other aspects of the covariance structure have not been examined, and changes to covariance and shape have not been compared directly.

To better understand the evolutionary lability of the **E** matrix, we used a set of induced mutations measured against a common co-isogenic wild type (Dworkin and Gibson 2006; Debat et al. 2009), as well as a panel of strains derived from natural populations, and examined the relationship between mean shape and different aspects of environmental covariance. Thus, all strains were reared under the same carefully-controlled conditions, and all mutant lines had the same genetic background, minimizing unknown sources of variation. We observe that mean shape varies more freely than the covariance structure, and that matrix orientation varies more than – and independently from – its size and eccentricity.

Material and Methods

Drosophila strains

Insertional mutations (caused by the insertion of P-elements, marked with w^+) in genes in the TGF-β and EGFR signaling pathways were provided from the Bloomington Stock Center (Table 1). These represent a subset of the alleles that were first described in Dworkin and Gibson (2006).

bioRxiv preprint doi: https://doi.org/10.1101/023333; this version posted July 27, 2015. The copyright holder for this preprint (which was not certified by peer review) is the author/funder, who has granted bioRxiv a license to display the preprint in perpetuity. It is made available under aCC-BY-NC 4.0 International license.

142 All insertions were initially introgressed into the wild-type lab strain Samarkand (Sam) for at least
143 10 generations. The Samarkand wild type was marked with w^- (white eyes) so flies with insertions
144 could be distinguished by a rescue of the eye color phenotype. Introgressions were performed by
145 repeated backcrossing of females bearing the insertion to males of Sam. Prior to generating flies
146 for the experiments described in this study, the alleles were backcrossed to Sam for an additional
147 four generations to remove any *de novo* mutations that had accumulated in these lines (relative
148 to Sam) since the original introgression procedure. Selection was based entirely on the presence
149 of the eye colour marker, precluding unwitting selection for wing phenotypes. All crosses were
150 performed using standard cornmeal-molasses media, in a 24° C Percival incubator on a 12/12-hr
151 light/dark cycle with 60% relative humidity (Dworkin and Gibson 2006). The mutant strains used
152 here are part of a larger unpublished study (Dworkin), and were chosen in part based on sample
153 size (>50/genotype).

154 **Experimental setup**

155 After the additional four generations of backcrossing back to Samarkand, crosses between
156 each mutation and Samarkand were set up in vials, allowing females to lay for 2-3 days, so that
157 egg density was low (generally less than 60 flies/vial). The temperature of the incubator was
158 maintained at 24° C, and monitored carefully for fluctuations, and vial position was randomized
159 within the incubator on a daily basis to reduce any possible edge effects. As larvae crawled out of
160 the media, a piece of paper towel was added to each vial to provide additional pupation space.
161 After eclosion and sclerotization flies were separated, on the basis of eye color, into wild-type
162 individuals without the P-element-induced mutations (w-) and heterozygotes for the P-element,
163 and then stored in 70% ethanol.

bioRxiv preprint doi: https://doi.org/10.1101/023333; this version posted July 27, 2015. The copyright holder for this preprint (which was not certified by peer review) is the author/funder, who has granted bioRxiv a license to display the preprint in perpetuity. It is made available under aCC-BY-NC 4.0 International license.

Strains derived from natural populations from North Carolina and Maine.

Iso-female lines of D. melanogaster were established separately in the summer of 2004 at a Peach orchard in West End, North Carolina (NC2) and in a blueberry field in Cherryfield Maine (courtesy of Marty Kreitman). To generate inbred lines, full-sib mating was performed for 15-20 generations (Goering et al 2009; Reed et al 2010). Flies were reared at 25C in a 12/12 light/dark cycle at 50% humidity. Seven Maine and five NC2 lines, each with at least 51 males were used here.

Data collection

A single wing from each fly was dissected and mounted in 70% glycerol (>20 wings per genotype/replicate on average; males only). Wings were imaged at 40X magnification on an Olympus DP30BW camera mounted on an Olympus BX51 microscope using 'DP controller' V3.1.1 software. All images were saved as greyscale tiff files. To extract landmark and semi-landmark data, we followed a modified protocol for the use of the "WINGMACHINE" software (Houle et al. 2003) as detailed in Pitchers et al. (2013). First, we used "tpsDig2" (Rohlf 2010) software to record the coordinates of the two starting landmarks needed by WINGMACHINE. We then used WINGMACHINE to automatically fit nine B-splines to the veins and margins of the wing (Fig. 2A). We reviewed each splined image and manually adjusted the control points as necessary. The x and y coordinates of 14 landmarks and 34 semi-landmarks (Fig. 2A) were extracted using CPR (Marquez and Houle 2014). The data were checked for visual outliers on scatter plots, and putative outliers were examined, and either fixed in WINGMACHINE or deleted. The resulting dataset was then passed on to **R** for further analysis.

Preparation of data

bioRxiv preprint doi: https://doi.org/10.1101/023333; this version posted July 27, 2015. The copyright holder for this preprint (which was not certified by peer review) is the author/funder, who has granted bioRxiv a license to display the preprint in perpetuity. It is made available under aCC-BY-NC 4.0 International license.

All specimens from all genotypes were superimposed together using Generalized Procrustes Analysis with function *gpagen* in the **R** package *geomorph 2.1.1* (Adams and Otarola-Castillo 2013). The semi-landmarks were optimized using minimum Procrustes distance. The whole dataset was then projected into the tangent space. Replicate effect was corrected by subtracting the replicate mean from each specimen and adding the grand mean of that genotype (Sokal and Rohlf 1995; Marroig and Cheverud 2004). The natural strains were similarly corrected for locality (Maine *vs.* North Carolina). Following these corrections, data were regressed on centroid size within each genotype, and added to the predicted value for that genotype mean size.

The size-regressed dataset was then passed on to LORY for calculating the interpolated Jacobian-based data (Marquez et al. 2012). LORY uses spatial interpolation to evaluate shape deformation at points throughout the wing. It starts by creating a tessellated grid, with the landmarks and semi-landmarks as the vertices (Fig. 3A). The centroids of the resulting triangles are considered the evaluation points. Given an interpolation function, it then calculates the Jacobian matrix that describes the shape deformation at each point (e.g., Fig. 3B). The log-transformed determinant of the Jacobian matrix quantifies the amount of expansion or contraction at each evaluation point relative to the mean configuration. Thus, the interpolation takes into account information from the whole configuration of landmarks, as well as from the rest of the sample through the mean configuration, while quantifying local shape changes. The resulting dataset is multivariate, rather than multidimensional, in the sense that each variable is meaningful in its own right and the whole dataset can be analyzed using conventional multivariate analyses (Marquez et al. 2012).

bioRxiv preprint doi: https://doi.org/10.1101/023333; this version posted July 27, 2015. The copyright holder for this preprint (which was not certified by peer review) is the author/funder, who has granted bioRxiv a license to display the preprint in perpetuity. It is made available under aCC-BY-NC 4.0 International license.

208 The interpolation function necessarily assumes a model for the distribution of shape
209 changes across the configuration. The most common interpolation function used in geometric
210 morphometrics studies is the Thin Plate Spline (TPS), which assumes the object is rigid and
211 therefore penalizes local deformations more than global ones. In this study we compared TPS
212 with another interpolation function implemented in LORY – the Elastic Body Spline (EBS) – that
213 assumes the object is elastic and penalizes local deformations less than global ones (Marquez et
214 al. 2012). Therefore, like the Procrustes superimposition, TPS tends to spread the variation more
215 globally than EBS. For this study system, we consider EBS to be a more suitable model *a priori*,
216 because the development of the fruit fly wing has been shown to proceed in a relatively
217 compartmentalized manner in which variation tends to be locally contained (Zecca and Struhl
218 2002; Barrio and Celis 2004; Cook et al. 2004; Martín and Morata 2006; Ziv et al. 2012). At the
219 same time, results based on Procrustes data were highly correlated with the Jacobian-based
220 data, using both TPS and EBS (Figs. S1-S2). Therefore, we chose to focus here on results based on
221 EBS. Results for TPS and Procrustes data are provided in the supplemental material. Each dataset
222 was reduced to its first 30 dimensions using Principal Component Analysis, covering 99% of the
223 variation in the data (Fig. S3). All subsequent analyses are based on these PCA scores.

224 **Quantification of variation and covariation**

225 Variance-covariance (VCV) matrices were quantified based on their size, orientation, and
226 shape (see Fig. 1). Matrix size was calculated as the trace of the matrix (i.e., total variance, or
227 sum of its eigenvalues). Matrix shape was characterized based on its eccentricity (Jones et al.
228 2003), and calculated as the ratio of the largest eigenvalue to the total variance, which is the
229 inverse of Kirkpatrick (2009)'s effective number of dimensions (Kirkpatrick 2009):

bioRxiv preprint doi: https://doi.org/10.1101/023333; this version posted July 27, 2015. The copyright holder for this preprint (which was not certified by peer review) is the author/funder, who has granted bioRxiv a license to display the preprint in perpetuity. It is made available under aCC-BY-NC 4.0 International license.

$$\text{Eccentricity} = \frac{\lambda_1}{\sum_{i=1}^{p} \lambda_i}$$

In addition, we calculated the relative standard deviation of the eigenvalues (rSDE), also known as integration level (Pavlicev et al. 2009; Haber 2011). However, rSDE yielded very similar results to the above measure of eccentricity (Fig. S4), and will not be considered further.

Similarity in matrix orientation was quantified using Random Skewers (Cheverud et al. 1983; Cheverud and Marroig 2007; Marroig et al. 2011), which measures the average similarity between two matrices in their response to random unit vectors (representing selection). We used 5000 random vectors drawn from a normal distribution with mean 0 and variance 1, normed to unit length (Marroig et al. 2011). A covariance distance metric was then calculated as $\sqrt{(1-r^2)}$, where r is the Random Skewers value for that pair of matrices, and normalized using Fisher's z-transformation (Jamniczky and Hallgrímsson 2009). Two other distance metrics were calculated as well: a modification of Krzanowski's (1979) metric following Zelditch et al. (2006), and the relative eigenvalues metric of Mitteroecker and Bookstein (2009). However, these two methods proved unstable for our dataset under resampling, yielding unreliable CI's. At the same time, their estimated values followed the same pattern as Random Skewers (see online supplementary material). Moreover, Random Skewers is the only method of the three that is related to evolutionary theory (Hansen and Houle 2008). Therefore, we present below only results based on Random Skewers.

Shape distances were calculated as the Euclidean distance for both the interpolated data and the Procrustes-based data, after projecting the Procrustes data to tangent space.

Confidence intervals for shape distances, matrix size, and eccentricity, were estimated

bioRxiv preprint doi: https://doi.org/10.1101/023333; this version posted July 27, 2015. The copyright holder for this preprint (which was not certified by peer review) is the author/funder, who has granted bioRxiv a license to display the preprint in perpetuity. It is made available under aCC-BY-NC 4.0 International license.

using a non-parametric bootstrap procedure with a BCa correction (DiCiccio and Efron 1996; Carpenter and Bithell 2000) using 999 iterations. The BCa correction was necessary because the pseudovalue distribution is expected to be biased upward when the statistic is bounded by zero, and to depend on its mean when bounded by both zero and one. These confidence intervals were used for evaluating significant differences as well.

Confidence intervals for covariance distance were estimated using a Jackknife procedure. Each Jackknife pseudovalue was calculated by leaving out one of the specimens in one of the two samples compared. The confidence interval was calculated as the 95% of the Jackknife distribution, without applying a bias correction. The Jackknife was preferred in this case because the bootstrap (both parametric and non-parametric) consistently resulted in distributions that were highly biased upward, often excluding the observed value, invalidating the BCa correction. This is a commonly found phenomenon in similar studies that has not yet been properly addressed in the literature to the best of our knowledge. Here we found that Jackknife without a bias correction provided fairy symmetric distributions around the observed values with reasonably wide confidence intervals, whereas the bias-corrected jackknife yielded extremely narrow intervals that often excluded their observed value (i.e., they were “over-corrected”).

In order to further compare covariance changes with shape changes we used Principal Coordinates Analysis to generate a shape space and a covariance space, based on all pairwise distances. Thus, in each of these spaces, genotypes are located based on how different they are from each other in either shape or matrix orientation. The covariance space was then superimposed onto the shape space using a symmetric Procrustes superimposition including scaling (function *protest* in **R** package *vegan 2.0-10*; Oksansen et al. 2013). The sum of squared

bioRxiv preprint doi: https://doi.org/10.1101/023333; this version posted July 27, 2015. The copyright holder for this preprint (which was not certified by peer review) is the author/funder, who has granted bioRxiv a license to display the preprint in perpetuity. It is made available under aCC-BY-NC 4.0 International license.

deviations between the two spaces, after superimposition, was used as a measure of correlation between them. In addition, we calculated the disparity of mutants and naturally-derived strains - for shape and covariance - as the sum of variances of their respective scores in the joint space. We used MANOVA (Pillai's Λ) to test the effect of pathway on the mutants' PCoA scores in both shape and covariance spaces.

All analyses were carried out in **R** 3.0.3. All scripts and data will be made available on DRYAD and on the Dworkin lab github repository.

Results

Both mean shape and matrix orientation vary considerably among mutant and naturally-derived strains.

All mutants and naturally-derived strains differ significantly in their mean shape from the Sam wild type (Table 2 and Fig. 4), as determined by the lack of overlap between their confidence intervals and the benchmark of zero distance from Sam (horizontal dashed line in figure 4). Most mutant strains are more similar to the Sam wild type than any of the naturally-derived strains. Yet, two of the mutants (*Omb*^{md653} and Bs^{k07909}) show magnitudes of shape change as extreme as any of the naturally derived strains, indicating that the range of mutations included here provide a reasonable representation of what we might observe in nature.

The orientation of the covariance matrix of all strains – mutants as well as naturally derived – also differ significantly from the Sam wild type (Table 2 and Fig. 5): none of the covariance distances include zero in their confidence interval. Unlike mean shape, however, most of the mutant strains differ from Sam just as much as the naturally-derived strains do.

bioRxiv preprint doi: https://doi.org/10.1101/023333; this version posted July 27, 2015. The copyright holder for this preprint (which was not certified by peer review) is the author/funder, who has granted bioRxiv a license to display the preprint in perpetuity. It is made available under aCC-BY-NC 4.0 International license.

295 ***Several mutant strains have lower environmental variance than their wild type***

296 Surprisingly, most mutations resulted in a lower total variance than their co-isogenic Sam
297 wild-type (Table 2 and Fig. 4). However, only 4 of the 12 mutant strains fall below the confidence
298 interval of Sam (Table 2). One of the significant strains ($tkv^{kg01923}$) is part of the TGF-β pathway,
299 and the other three (S^{k09530}, $rho^{kg07115}$, spi^{s3547}) contribute to EGFR signaling (Table 1). The only
300 strain that has substantially and significantly higher total variance is Omb^{md653}, which also differs
301 greatly in its mean shape. The variance within each of the naturally-derived strains is mostly
302 higher than that of Sam, but only 3 of the 12 naturally-derived strains are above the confidence
303 interval of Sam. In addition, there is a positive linear relationship between the total variance
304 within each mutant strain and its shape distance from Sam across the mutant strains (Fig. 4). This
305 is consistent with the common expectation that greater decanalization is associated with larger
306 changes to mean shape.
307
308 ***A positive non-linear association between changes in mean shape and matrix***
309 ***orientation***.
310 There is also a weak, but positive association between covariance distance (orientation)
311 and shape distance (Fig. 5), relative to the Sam wild type. This relationship, however, is not linear,
312 suggesting that the covariance distance is somewhat bounded at the upper range. These findings
313 are further supported by comparing the shape and covariance PCoA spaces (Fig. 6). These spaces
314 are based on all pairwise comparisons, rather than comparing to Sam only, and were
315 superimposed for comparability. The Procrustes superimposition scales the two spaces to a
316 common scale, centers, and rotates them so that they are comparable in terms of both

bioRxiv preprint doi: https://doi.org/10.1101/023333; this version posted July 27, 2015. The copyright holder for this preprint (which was not certified by peer review) is the author/funder, who has granted bioRxiv a license to display the preprint in perpetuity. It is made available under aCC-BY-NC 4.0 International license.

magnitude and direction of change. The grey solid lines indicate the deviation between the two spaces. The Procrustes sum of squares 0.669, and the coefficient of determination between the two spaces is small yet significantly different from zero (R^2 = 0.33; p≤0.001 with 999 permutations). Thus, the two spaces are substantially different from each other, but not unrelated. The first PCo1 axis mostly separates the naturally-derived strains from the mutants+Sam, for both shape and covariance. The disparity of shape is more than twice as large as that of the covariance structure when strain *Omb*^{md653} is included, and twice as large when it is excluded (Table 3; calculations include all 24 PCoA dimensions that resulted in eigenvalues larger than zero). The disparity of both shape and covariance is larger for the naturally-derived strains than for the mutants, both with and without *Omb*^{md653}. The mutants do not cluster by pathway (Fig. 6B), for either shape (Pillai's Λ=0.44, p=0.24) or covariance distance (Pillai's Λ=0.34, p=0.52).

Most mutations do not influence matrix eccentricity, despite effects on mean shape, matrix size, and matrix orientation.

Most of the mutations do not have a substantial effect on the eccentricity of the matrix (i.e., matrix shape). Most values fall well within the confidence interval of their co-isogenic Sam wild type (Table 2). The only mutation that made a substantial (and significant) increase in eccentricity is *aos*^{W11}. Interestingly, *aos*^{W11} does not differ much from Sam for total variance (Fig. 7A). *Omb*^{md653}, on the other hand, differs significantly and substantially from Sam in its total variance and shape (see Table 2), and yet is very similar in its eccentricity to Sam. Most of the naturally-derived strains have a higher eccentricity than Sam (Fig. 7A), showing a greater difference from Sam than the mutants do, as well as a slight tendency toward a positive association with the total variance. However, this association depends mostly on the two most

bioRxiv preprint doi: https://doi.org/10.1101/023333; this version posted July 27, 2015. The copyright holder for this preprint (which was not certified by peer review) is the author/funder, who has granted bioRxiv a license to display the preprint in perpetuity. It is made available under aCC-BY-NC 4.0 International license.

339 deviating strains. When eccentricity is calculated using the relative standard deviation of the
340 eigenvalues (rSDE), a few additional strains differ significantly from Sam (Table 2), but the
341 relationship between eccentricity and total variance is still weak (Fig. S12). Similarly, there is no
342 clear association between eccentricity and shape distance from Sam (figure 7B), and no
343 relationship between eccentricity and covariance distance from Sam (Fig. 7C). The same picture
344 emerges using other metrics of covariance distance, based on both Procrustes and TPS data (Figs.
345 S10-S11).
346
347 Discussion
348 The pattern and magnitude of phenotypic covariation remains central to selection theory
349 (Robertson 1966; Price 1970; Lande and Arnold 1983). Although it cannot facilitate adaptation,
350 the environmental component of phenotypic covariation, **E**, can impede and divert the
351 population response to selection (Burger 1986). Despite the importance of this for our
352 understanding the response to selection, factors that influence the lability of **E** are poorly
353 understood. For univariate measures, environmental and genetic stressors have been shown to
354 increase variance in **E** in numerous situations (Dworkin 2005; Hallgrímsson et al. 2009; Paaby and
355 Rockman 2014; and references therein), but little is known about how such perturbations
356 influence other properties of integration and covariation.
357 Using the wing of *Drosophila melanogaster* as a model system, we found that mean shape
358 and matrix orientation vary among the co-isogenic mutants, as well as the naturally-derived
359 strains (Table 1 and Fig. 5). By superimposing the covariance space onto shape space we were
360 able to compare their distribution in terms of both magnitude and direction of change and show

bioRxiv preprint doi: https://doi.org/10.1101/023333; this version posted July 27, 2015. The copyright holder for this preprint (which was not certified by peer review) is the author/funder, who has granted bioRxiv a license to display the preprint in perpetuity. It is made available under aCC-BY-NC 4.0 International license.

that shape has changed to a greater extent than matrix orientation (Fig. 6). In contrast, mutations had little influence on the total variance and eccentricity of the matrix. Whereas total variance is positively associated with mean shape, it is not associated with eccentricity, nor is eccentricity associated with matrix orientation. All together, these findings suggest that the potential of the covariance structure to change is more limited than that of mean shape, and that different properties of the covariance structure can change independently from each other. It is worth noting that some of the environmental effects (such as rearing temperature and density) were highly controlled in this study, both within and among strains. Thus, our experimental design may represent a lower bound for the environmental contributions to covariation, and the patterns observed are likely an underestimate of the possible effect sizes.

Contrary to the common expectation (Dworkin 2005; Hallgrímsson et al. 2009; and references therein), the variance of most mutants decreases relative to their co-isogenic wild type, Samarkand (Sam) (albeit significant for only 4/12 genotypes). Equally puzzling is the observation that the natural strains all have higher variance than Sam rather than distributed around Sam. Since the individuals within each strain are genetically identical, the decrease in total variance within the mutants, and the increase within the natural strains, likely reflects a higher, and lower, canalization of wing shape, respectively (Hall et al 2007). Such mixed results have been observed also by Dworkin and Gibson (2006) for mutant strains, using a smaller set of landmarks. A related study (Debat et al 2009) showed a more consistent increase in total variance, even for some of the same mutations. However, the genetic background of the wild type strains in Debat et. al (2009) was Oregon-R (rather than Samarkand), which has been shown to be more sensitive to mutational perturbations under some conditions (Chari & Dworkin 2013).

bioRxiv preprint doi: https://doi.org/10.1101/023333; this version posted July 27, 2015. The copyright holder for this preprint (which was not certified by peer review) is the author/funder, who has granted bioRxiv a license to display the preprint in perpetuity. It is made available under aCC-BY-NC 4.0 International license.

Increases in the environmental component of phenotypic variance have been explained in previous studies by a nonlinear relationship between the trait mean and its underlying developmental parameters (Klingenberg and Nijhout 1999; Hallgrímsson et al. 2009). A steeper slope for relationship between underlying developmental parameters and phenotypic variation implies greater variation is expressed around the mean phenotype, and therefore a less canalized phenotype. It often assumed that the wild type is at its most canalized state, and therefore when development is perturbed the mean is expected to shift to a less canalized section on the curve and express greater variation. It is possible, however, that the mean would shift into more canalized regions, rather than less canalized, resulting in a decrease of variance rather than an increase. It is also possible to have system-wide canalizing factors (such as chaperon proteins; Rutherford and Lindquist 1998) operate simultaneously, masking the effects of local perturbations and stabilizing the variance (Hallgrímsson et al. 2006). Or, the mutations could increase redundancy and complexity thus increasing stability (Hallgrímsson et al. 2006; Levy and Siegal 2008). All of these possible explanations would be consistent with the relationship we found between changes of mean shape and total variance (relative to the Sam co-isogenic wild type).

A possible explanation for the increase in variance within the natural strains could be related to the time and amount of inbreeding among the strains (Whitlock & Fowler 1999; Whitlock et al. 2002). Inbreeding in *Drosophila* does represent a form of “genetic stress” as deleterious recessive alleles are made homozygous (and their effects are phenotypically expressed). We would therefore expect the natural strains to be de-canalized as well. However,

bioRxiv preprint doi: https://doi.org/10.1101/023333; this version posted July 27, 2015. The copyright holder for this preprint (which was not certified by peer review) is the author/funder, who has granted bioRxiv a license to display the preprint in perpetuity. It is made available under aCC-BY-NC 4.0 International license.

404 the Sam wild-type has also undergone very extensive inbreeding, and is near isogenic (Chandler
405 et al. 2014). Thus, a satisfactory explanation for this particular observation eludes us.

406 In accord with previous studies (Dworkin and Gibson 2006; Debat et al. 2009; Jamniczky
407 and Hallgrímsson 2009), covariance matrices of the mutant strains do not cluster according to the
408 developmental pathway that they presumably affect. This could points to the complexity of the
409 developmental system, further supporting the palimpsest model suggested by Hallgrímsson et al.
410 (2009). It could also mean that these pathways do not contribute to the structure of **E** as
411 effectively and consistently as previously postulated. A detailed analysis of the covariance
412 pattern is needed to further investigate the extent to which the modularity structure of the fruit
413 fly wing follows *a priori* developmental models, and how it is disrupted by developmental
414 perturbations.

415 It is difficult to compare differences in eccentricity to differences in orientation directly
416 because of their different dimensionality and somewhat different method for calculating CI's.
417 However, mutant eccentricity varies from that of Sam within a smaller portion of its possible
418 range (0.2-0.43; 23%) compared to how much their orientation varies from Sam (0.37-0.77; 40%
419 without the Fisher's *z*-transformation). These findings are in accord with simulations by Jones et
420 al. (2003, 2004, 2012) for **G**, suggesting that eccentricity is likely to vary less than orientation for
421 a given population size under most combinations of genetic architecture, selection regimes, and
422 phylogenetic scale. It is also consistent with empirical evidence for **P** from Haber (2015a,b),
423 showing that matrix orientation has varied greatly among closely-related ruminant species,
424 whereas eccentricity has remained largely the same throughout most of bovids history, and only
425 varied within 33% of its possible range among other ruminants.

bioRxiv preprint doi: https://doi.org/10.1101/023333; this version posted July 27, 2015. The copyright holder for this preprint (which was not certified by peer review) is the author/funder, who has granted bioRxiv a license to display the preprint in perpetuity. It is made available under aCC-BY-NC 4.0 International license.

426 Previous studies have shown an increase in variance to be clearly associated with
427 decanalization. In this study, however, we find that mutants altered the orientation of the
428 covariance matrix more often than its total variance. Mutations do not only affect trait means
429 and variances, but aspects of covariances as well, though this has not been part of the general
430 formulation so far. Thus, our study suggests that it might be useful to consider a more general
431 concept of decanalization.
432
433 **Acknowledgements**: We thank Ellen Larsen, Jeff Conner and Will Pitchers for comments
434 that improved clarity of this manuscript. This material is based in part on work supported by the
435 National Science Foundation under Cooperative Agreement No. DBI-0939454. Any opinions,
436 findings and conclusions or recommendations expressed in this material are those of the
437 author(s) and do not necessarily reflect the views of the National Science Foundation. This work
438 was supported by NIH grant 1R01GM094423-01 to ID. Funding for AH was provided by the
439 Council of Higher Education, Israel, and BEACON Center for the Study of Evolution in Action at
440 Michigan State University.
441

bioRxiv preprint doi: https://doi.org/10.1101/023333; this version posted July 27, 2015. The copyright holder for this preprint (which was not certified by peer review) is the author/funder, who has granted bioRxiv a license to display the preprint in perpetuity. It is made available under aCC-BY-NC 4.0 International license.

441 Literature cited

442 Adams, D. C., and E. Otarola-Castillo. 2013. geomorph: an R package for the collection and
443 analysis of geometric morphometric shape data. Methods in Ecology and Evolution 4:393-
444 399.

445 Arnold, S. J., R. Burger, P. A. Hohenlohe, B. C. Ajie, and A. G. Jones. 2008. Understanding the
446 evolution and stability of the G-matrix. Evolution 62:2451-2461.

447 Arnold, S. J., R. Bürger, P. A. Hohenlohe, B. C. Ajie, and A. G. Jones. 2008. Understanding the
448 evolution and stability of the G-matrix. Evolution 62:2451-2461.

449 Barrio, R., and C. de, Jose F. 2004. Regulation of *spalt* expression in the *Drosophila* wing blade in
450 response to the Decapentaplegic signaling pathway. Proceedings of the National Academy
451 of Sciences of the United States of America 101:6021-6026.

452 Breuker, C. J., J. S. Patterson, and C. P. Klingenberg. 2006. A Single Basis for Developmental
453 Buffering of *Drosophila* Wing Shape. PLoS ONE 1:e7.

454 Burger, R. 1986. Constraints for the evolution of functionally coupled characters: A nonlinear
455 analysis of a phenotypic model. Evolution 40:182-193.

456 Camara, M., C. Ancell, and M. Pigliucci. 2000. Induced mutations: a novel tool to study
457 phenotypic integration and evolutionary constraints in *Arabidopsis thaliana*. Evolutionary
458 Ecology Research 2:1009-1029.

459 Carpenter, J., and J. Bithell. 2000. Bootstrap confidence intervals: when, which, what? A
460 practical guide for medical statisticians. Statistics in Medicine 19:1141-1164.

461 Chari, S., and I. Dworkin. 2013. The Conditional Nature of Genetic Interactions: The
462 Consequences of Wild-Type Backgrounds on Mutational Interactions in a Genome-Wide

bioRxiv preprint doi: https://doi.org/10.1101/023333; this version posted July 27, 2015. The copyright holder for this preprint (which was not certified by peer review) is the author/funder, who has granted bioRxiv a license to display the preprint in perpetuity. It is made available under aCC-BY-NC 4.0 International license.

463 Modifier Screen. PLoS Genetics 9:e1003661.

464 Chandler, C. H., S. Chari, D. Tack, and I. Dworkin. 2014. Causes and Consequences of Genetic

465 Background Effects Illuminated by Integrative Genomic Analysis. Genetics 196:1321-1336.

466 Cheverud, J. M., J. J. Rutledge, and W. R. Atchley. 1983. Quantitative Genetics of Development:

467 Genetic Correlations Among Age-Specific Trait Values and the Evolution of Ontogeny.

468 Evolution 37:895-905.

469 Cook, O., B. Biehs, and E. Bier. 2004. *brinker* and *optomotor-blind* act coordinately to initiate

470 development of the L5 wing vein primordium in *Drosophila*. Development 131:2113-2124.

471 de Oliveira, F. B., A. Porto, and G. Marroig. 2009. Covariance structure in the skull of Catarrhini:

472 a case of pattern stasis and magnitude evolution. Journal of Human Evolution 56:417-430.

473 Debat, V., S. Bloyer, F. Faradji, N. Gidaszewski, N. Navarro, P. Orozco-terWengel, V. Ribeiro, C.

474 Schlötterer, J. S. Deutsch, and F. Peronnet. 2011. Developmental Stability: A Major Role

475 for *Cyclin G* in *Drosophila melanogaster*. PLoS Genetics 7:e1002314.

476 Debat, V., A. Debelle, and I. Dworkin. 2009. Plasticity, canalization, and developmental stability

477 of the *Drosophila* wing: joint effects of mutations and developmental temperature.

478 Evolution 63:2864-2876.

479 Debat, V., C. C. Milton, S. Rutherford, C. P. Klingenberg, and A. A. Hoffmann. 2006. Hsp90 and

480 the quantitative variation of wing shape in *Drosophila melanogaster*. Evolution 60:2529-

481 2538.

482 DiCiccio, T. J., and B. Efron. 1996. Bootstrap Confidence Intervals. Statistical Science 11:189-212.

483 Dworkin, I. 2005a. A study of canalization and developmental stability in the sternopleural

484 bristle system of *Drosophila melanogaster*. Evolution 59:1500-1509.

bioRxiv preprint doi: https://doi.org/10.1101/023333; this version posted July 27, 2015. The copyright holder for this preprint (which was not certified by peer review) is the author/funder, who has granted bioRxiv a license to display the preprint in perpetuity. It is made available under aCC-BY-NC 4.0 International license.

485 Dworkin, I. 2005b. Canalization, cryptic variation, and developmental buffering: a critical
486 examination and analytical perspective. Pp. 131-158 *in* B. Hallgrímsson and B. K. Hall, eds.
487 Variation, a central concept in biology
488 Dworkin, I., and G. Gibson. 2006. The EGF-R and TGF-ß signal transduction pathways contribute
489 to variation for wing shape in *Drosophila melanogaster*. Genetics 173:1417–1431.
490 Goering, L. M., P. K. Hunt, C. Heighington, C. Busick, P. Pennings, J. Hermisson, S. Kumar, and G.
491 Gibson. 2009. Association of orthodenticle with natural variation for early embryonic
492 patterning in *Drosophila melanogaster*. Journal of Experimental Zoology Part B: Molecular
493 and Developmental Evolution 312B:841-854.
494 Haber, A. 2011. A Comparative Analysis of Integration Indices. Evolutionary Biology 38:476-488.
495 Haber, A. 2015a. The Evolution of Morphological Integration in the Ruminant Skull. Evolutionary
496 Biology 42:99-114.
497 Haber, A. 2015b. Phenotypic Covariation And Morphological Diversification In The Ruminant
498 Skull. bioRxiv doi: http://dx.doi.org/10.1101/017533.
499 Hall, M. C., I. Dworkin, M. C. Ungerer, and M. Purugganan. 2007. Genetics of
500 microenvironmental canalization in *Arabidopsis thaliana*. Proceedings of the National
501 Academy of Sciences 104:13717.
502 Hallgrímsson, B., H. A. Jamniczky, N. Young, C. Rolian, T. Parsons, J. Boughner, and R. Marcucio.
503 2009. Deciphering the Palimpsest: Studying the Relationship Between Morphological
504 Integration and Phenotypic Covariation. Evolutionary Biology 36:355-376.
505 Hallsson, L. R., and M. Björklund. 2012. Selection in a fluctuating environment leads to
506 decreased genetic variation and facilitates the evolution of phenotypic plasticity. Journal

bioRxiv preprint doi: https://doi.org/10.1101/023333; this version posted July 27, 2015. The copyright holder for this preprint (which was not certified by peer review) is the author/funder, who has granted bioRxiv a license to display the preprint in perpetuity. It is made available under aCC-BY-NC 4.0 International license.

of Evolutionary Biology 25:1275-1290.

Hansen, T. F., and D. Houle. 2008. Measuring and comparing evolvability and constraint in multivariate characters. Journal of Evolutionary Biology 21:1201-1219.

Hohenlohe, P. A., and S. J. Arnold. 2008. MIPoD: A Hypothesis-Testing Framework for Microevolutionary Inference from Patterns of Divergence. The American Naturalist 171:366-385.

Houle, D., J. Mezey, P. Galpern, and A. Carter. 2003. Automated measurement of Drosophila wings. BMC Evolutionary Biology 3:25.

Jamniczky, H. A., and B. Hallgrímsson. 2009. A Comparison of Covariance Structure in Wild and Laboratory Muroid Crania. Evolution 63:1540-1556.

Jones, A. G., S. J. Arnold, and R. Bürger. 2003. Stability of the G-Matrix in a Population Experiencing Pleiotropic Mutation, Stabilizing Selection, and Genetic Drift. Evolution 57:1747-1760.

Jones, A. G., S. J. Arnold, and R. Bürger. 2004. Evolution and Stability of the G-Matrix on a Landscape with a Moving Optimum. Evolution 58:1639-1654.

Jones, A. G., S. J. Arnold, R. Bürger, and C. Goodnight. 2007. The mutation matrix and the evolution of evolvability. Evolution 61:727-745.

Jones, A. G., R. Bürger, S. J. Arnold, P. A. Hohenlohe, and J. C. Uyeda. 2012. The effects of stochastic and episodic movement of the optimum on the evolution of the G-matrix and the response of the trait mean to selection. Journal of Evolutionary Biology 25:2210-2231.

Kirkpatrick, M. 2009. Patterns of quantitative genetic variation in multiple dimensions. Genetica 136:271-284.

bioRxiv preprint doi: https://doi.org/10.1101/023333; this version posted July 27, 2015. The copyright holder for this preprint (which was not certified by peer review) is the author/funder, who has granted bioRxiv a license to display the preprint in perpetuity. It is made available under aCC-BY-NC 4.0 International license.

529 Klingenberg, C. P., and H. F. Nijhout. 1999. Genetics of Fluctuating Asymmetry: A Developmental
530 Model of Developmental Instability. Evolution 53:358-375.
531 Lande, R. 1979. Quantitative Genetic Analysis of Multivariate Evolution, Applied to Brain: Body
532 Size Allometry. Evolution 33:402-416.
533 Lande, R., and S. J. Arnold. 1983. The measurement of selection on correlated characters.
534 Evolution 37:1210-1226.
535 Le Rouzic, A., J. Álvarez-Castro, and T. F. Hansen. 2013. The Evolution of Canalization and
536 Evolvability in Stable and Fluctuating Environments. Evol Biol Evolutionary Biology 40:317-
537 340.
538 Ledón-Rettig, C. C., D. W. Pfennig, A. J. Chunco, and I. Dworkin. 2014. Cryptic Genetic Variation
539 in Natural Populations: A Predictive Framework. Integrative and Comparative Biology
540 54:783-793.
541 Levy, S. F., and M. L. Siegal. 2008. Network Hubs Buffer Environmental Variation in
542 *Saccharomyces cerevisiae*. PLoS Biology 6:e264.
543 Marquez, E. J., R. Cabeen, R. P. Woods, and D. Houle. 2012. The Measurement of Local Variation
544 in Shape. Evolutionary Biology 39:419-439.
545 Marroig, G., and J. M. Cheverud. 2004. Cranial evolution in sakis (*Pithecia*, Platyrrhini) I:
546 Interspecific differentiation and allometric patterns. American Journal of Physical
547 Anthropology 125:266-278.
548 Marroig, G., D. Melo, A. Porto, H. Sebastião, and G. Garcia. 2011. Selection Response
549 Decomposition (SRD): A New Tool for Dissecting Differences and Similarities Between
550 Matrices. Evolutionary Biology 38:225-241.

bioRxiv preprint doi: https://doi.org/10.1101/023333; this version posted July 27, 2015. The copyright holder for this preprint (which was not certified by peer review) is the author/funder, who has granted bioRxiv a license to display the preprint in perpetuity. It is made available under aCC-BY-NC 4.0 International license.

551 Martín, F. A., and G. Morata. 2006. Compartments and the control of growth in the Drosophila
552 wing imaginal disc. Development 133:4421-4426.
553 Mitteroecker, P., and F. Bookstein. 2009. The ontogenetic trajectory of the phenotypic
554 covariance matrix, with examples from craniofacial shape in rats and humans. Evolution
555 63:727-737.
556 Oksanen, J., F. G. Blanchet, R. Kindt, P. Legendre, P. R. Minchin, R. G. O'Hara, G. L. Simpson, P.
557 Solymos, H. M. H. Stevens, and H. Wagner. 2013. *vegan*: Community Ecology Package.
558 Paaby, A. B., and M. V. Rockman. 2014. Cryptic genetic variation: evolution's hidden substrate.
559 Nature Reviews Genetics 15:247-258.
560 Pavlicev, M., J. Cheverud, and G. Wagner. 2009. Measuring Morphological Integration Using
561 Eigenvalue Variance. Evolutionary Biology 36:157-170.
562 Pitchers, W, Pool, JE, Dworkin, I: Altitudinal clinal variation in wing size and shape in African
563 *Drosophila melanogaster*: one cline or many? Evolution 2013, 67:438–452
564 Porto, A., F. de Oliveira, L. Shirai, V. De Conto, and G. Marroig. 2009. The Evolution of
565 Modularity in the Mammalian Skull I: Morphological Integration Patterns and Magnitudes.
566 Evolutionary Biology 36:118-135.
567 Price, G. R. 1970. Selection and covariance. Nature 227:520-521.
568 Reed, L. K., S. Williams, M. Springston, J. Brown, K. Freeman, C. E. DesRoches, M. B. Sokolowski,
569 and G. Gibson. 2010. Genotype-by-Diet Interactions Drive Metabolic Phenotype
570 Variation in *Drosophila melanogaster*. Genetics 185:1009-1019.
571 Revell, L. J. 2007. The G matrix under fluctuating correlational mutation and selection. Evolution
572 61:1857-1872.

bioRxiv preprint doi: https://doi.org/10.1101/023333; this version posted July 27, 2015. The copyright holder for this preprint (which was not certified by peer review) is the author/funder, who has granted bioRxiv a license to display the preprint in perpetuity. It is made available under aCC-BY-NC 4.0 International license.

573 Robertson, A. 1966. A mathematical model of the culling process in dairy cattle. Animal Science
574 8:95-108.
575 Rohlf, F. 2010. tpsDig, digitize landmarks and outlines. 2.16. Department of ecology and
576 evolution. Stony Brook: State University
577 Rutherford, S. L., and S. Lindquist. 1998. Hsp90 as a capacitor for morphological evolution.
578 Nature 396:336-342.
579 Sokal, R. R., and F. J. Rohlf. 1995. Biometry. W. H. Freeman and company, New York.
580 Vermeij, G. J. 1973. Adaptation, Versatility, and Evolution. Systematic Zoology 22:466-477.
581 Waddington, C. H. 1952. Selection of the Genetic Basis for an Acquired Character. Nature
582 169:625-626.
583 Weber, K., N. Johnson, D. Champlin, and A. Patty. 2005. Many P-Element Insertions Affect Wing
584 Shape in *Drosophila melanogaster*. Genetics 169:1461-1475.
585 Willmore, K. E., C. P. Klingenberg, and B. Hallgrímsson. 2005. The relationship between
586 fluctuating asymmetry and environmental variance in rhesus macaque skulls. Evolution
587 59:898-909.
588 Willmore, K. E., N. M. Young, and J. T. Richtsmeier. 2007. Phenotypic Variability: Its
589 Components, Measurement and Underlying Developmental Processes. Evolutionary
590 Biology Evolutionary Biology 34:99-120.
591 Whitlock, M. C., P. C. Phillips, and K. Fowler. 2002. Persistence of changes in the genetic
592 covariance matrix after a bottleneck. Evolution 56:1968-1975.
593 Whitlock, M. C., and K. Fowler. 1999. The Changes in Genetic and Environmental Variance With
594 Inbreeding in *Drosophila melanogaster*. Genetics 152:345-353.

bioRxiv preprint doi: https://doi.org/10.1101/023333; this version posted July 27, 2015. The copyright holder for this preprint (which was not certified by peer review) is the author/funder, who has granted bioRxiv a license to display the preprint in perpetuity. It is made available under aCC-BY-NC 4.0 International license.

595 Zecca, M., and G. Struhl. 2002. Subdivision of the *Drosophila* wing imaginal disc by EGFR-
596 mediated signaling. Development 129:1357-1368.
597 Zelditch, M. L., J. Mezey, H. D. Sheets, B. L. Lundrigan, and G. J. Theodore. 2006. Developmental
598 regulation of skull morphology II: ontogenetic dynamics of covariance. Evolution &
599 Development 8:46-60.
600 Ziv, O., R. Finkelstein, Y. Suissa, T. Dinur, G. Deshpande, and O. Gerlitz. 2012. Inverse regulation
601 of target genes at the brink of the BMP morphogen activity gradient. Journal of Cell
602 Science 125:5811-5818.
603

bioRxiv preprint doi: https://doi.org/10.1101/023333; this version posted July 27, 2015. The copyright holder for this preprint (which was not certified by peer review) is the author/funder, who has granted bioRxiv a license to display the preprint in perpetuity. It is made available under aCC-BY-NC 4.0 International license.

603
604 Figures

605 Figure 1: Illustration of the different matrix properties. Ellipses represent 95% confidence interval
606 of a normal bivariate distribution, and arrows (ellipse axes) represent orthogonal axes of
607 covariaton. Matrices are presented as bivariate for illustration, but the principles are the same
608 for multivariate. Ellipses A, B, and C represent a change in only one property each, relative to the
609 ellipse in the middle. **A**, smaller matrix size (lower total variance); **B**, perpendicular orientation; **C**,
610 higher eccentricity.

611

612 Figure 2: **A,** A representative wing image with fitted splines and the location of landmarks and
613 semilandmarks along them. **B,** Individual variation in the sample (grey) relative to Sam (black),
614 mutant means (green), and means for naturally-derived lines (red).

615

616 Figure 3: Illustrating the LORY method for interpolating shape changes from Procrustes data of
617 genotype Bs^{k07909}. **A**, the tessellation scheme for choosing evaluation points. The landmarks and
618 semi-landmarks (dots) are used as vertices. The centroids of the resulting triangles (crosses) are
619 the final evaluation points. **B**, shape differences between the genotype mean and Sam inferred
620 by calculating the Jacobians around each evaluation point, scaled by 100 (crosses and crossed
621 circles). Bars represent the direction and change of differences between Sam and the sample
622 mean at the landmarks and semi-landmarks based on the Procrustes data, scaled by 10X.

623

624 Figure 4: Mean-shape distance from Sam plotted against the total variance within each strain.
625 Bars are 95% confidence intervals. Dashed lines represent values for the Sam wild type.

bioRxiv preprint doi: https://doi.org/10.1101/023333; this version posted July 27, 2015. The copyright holder for this preprint (which was not certified by peer review) is the author/funder, who has granted bioRxiv a license to display the preprint in perpetuity. It is made available under aCC-BY-NC 4.0 International license.

626

627 Figure 5: Covariance distance (i.e orientation differences), estimated by Random Skewers,

628 plotted against mean-shape distance, relative to the Sam wild type.

629

630 Figure 6: Covariance space superimposed onto shape space. Both spaces are based on all

631 pairwise distances. Solid grey lines indicate the deviation between the two spaces for a given

632 genotype. **A,** All genotypes; **B,** Mutants only, including the Sam wild type. Mutants that affect the

633 TGF-β pathway are marked by *t*. All other mutants affect the EGFR pathway

634

635 Figure 7: The association between eccentricity and total variance within each genotype (**A**), their

636 mean-shape distance from Sam (**B**) and their covariance distance from Sam (**C**)

637

638

bioRxiv preprint doi: https://doi.org/10.1101/023333; this version posted July 27, 2015. The copyright holder for this preprint (which was not certified by peer review) is the author/funder, who has granted bioRxiv a license to display the preprint in perpetuity. It is made available under aCC-BY-NC 4.0 International license.

Table 1: Information about the genotypes included in this study

Genotype	N	Wild Type	Allele	Gene		Pathway
Sam	175	Sam	Wild type	Wild type		-
10385	81	Sam	k05115	*Epidermal growth factor Receptor*	$Egfr^{k05115}$	Egfr
10413	88	Sam	k07909	*Blistered*	Bs^{k07909}	Egfr
10418	84	Sam	k09530	*Star*	S^{k09530}	Egfr
10462	89	Sam	s3547	*spitz*	spi^{s3547}	Egfr
10514	83	Sam	k02507	*Patched*	Ptc^{k02507}	Hh
12772	90	Sam	BG01610	*scribbler*	$sbb^{BG01610}$	TGF-β
14321	89	Sam	kg07115	*rhomboid*	$rho^{kg07115}$	Egfr
14403	76	Sam	kg01923	*thickveins*	$tkv^{kg01923}$	TGF-β
2513	86	Sam	W11	*argos*	aos^{W11}	Egfr
3045	92	Sam	md653	*Optometer blind/Bifid*	Omb^{md653}	TGF-β
6342	92	Sam	225-3	*crossveinless-2*	$cv\text{-}2^{225\text{-}3}$	TGF-β
6372	82	Sam	mip-w[+]	*GTPase activating protein1*	$Gap1^{mip\text{-}w[+]}$	Egfr
MA10	63	MA	WT	WT	-	-
MA12	62	MA	WT	WT	-	-
MA44	52	MA	WT	WT	-	-
MA53	55	MA	WT	WT	-	-
MA61	56	MA	WT	WT	-	-
MA70	57	MA	WT	WT	-	-
MA71	55	MA	WT	WT	-	-
NC2	54	NC	WT	WT	-	-
NC30	51	NC	WT	WT	-	-
NC53	58	NC	WT	WT	-	-
NC9	51	NC	WT	WT	-	-
NC94	61	NC	WT	WT	-	-

bioRxiv preprint doi: https://doi.org/10.1101/023333; this version posted July 27, 2015. The copyright holder for this preprint (which was not certified by peer review) is the author/funder, who has granted bioRxiv a license to display the preprint in perpetuity. It is made available under aCC-BY-NC 4.0 International license.

Table 2: Matrix properties of all genotypes, and their distance from Sam in terms of matrix orientation (cov.dis) and mean shape (shape.dis). All measures are based on Jacobians, using EBS, and are therefore proportional to the mean configuration of that genotype.

Genotype	Total variance	rSDE	Eccentricity[a]	cov.dis[b]	shape.dis
Sam (wild type)	0.13 (0.12,0.15)	0.28 (0.26,0.29)	0.23 (0.19,0.26)	0	0
aos^{W11}	0.12 (0.11,0.15)	*0.35 (0.29,0.41)	*0.34 (0.25,0.42)	*0.54 (0.53,0.55)	*0.25 (0.22,0.29)
Omb^{md653}	*0.18 (0.16,0.21)	0.29 (0.26,0.29)	0.21 (0.18,0.23)	*0.68 (0.67,0.68)	*1.23 (1.19,1.27)
cv-2$^{225-3}$	0.12 (0.1,0.14)	0.29 (0.28,0.3)	0.23 (0.19,0.26)	*0.44 (0.44,0.45)	*0.22 (0.18,0.25)
Gap1$^{mip-w[+]}$	0.12 (0.11,0.15)	*0.31 (0.28,0.32)	0.24 (0.19,0.3)	*0.65 (0.64,0.66)	*0.43 (0.38,0.46)
Egfr^{k05115}	0.12 (0.11,0.14)	*0.31 (0.28,0.31)	0.25 (0.21,0.28)	*0.52 (0.51,0.53)	*0.23 (0.2,0.26)
Bs^{k07909}	0.13 (0.12,0.15)	*0.30 (0.27,0.31)	0.26 (0.2,0.3)	*0.56 (0.55,0.57)	*0.63 (0.6,0.65)
S^{k09530}	*0.10 (0.09,0.12)	0.29 (0.27,0.3)	0.23 (0.19,0.27)	*0.42 (0.41,0.43)	*0.13 (0.1,0.14)
spl^{s3547}	*0.11 (0.10,0.12)	0.29 (0.27,0.29)	0.24 (0.19,0.28)	*0.50 (0.5,0.51)	*0.38 (0.34,0.41)
Ptc^{k02507}	0.12 (0.11,0.14)	0.29 (0.27,0.29)	0.20 (0.18,0.21)	*0.55 (0.54,0.56)	*0.53 (0.5,0.56)
sbb^{BG01610}	0.13 (0.11,0.15)	*0.30 (0.28,0.31)	0.25 (0.19,0.3)	*0.52 (0.52,0.53)	*0.37 (0.34,0.4)
rho^{kg07115}	*0.10 (0.1,0.12)	0.29 (0.27,0.29)	0.22 (0.18,0.25)	*0.39 (0.39,0.4)	*0.17 (0.14,0.19)
tkv^{kg01923}	*0.10 (0.09,0.12)	*0.30 (0.28,0.3)	0.23 (0.19,0.25)	*0.60 (0.59,0.61)	*0.3 (0.27,0.33)
MA10	0.15 (0.13,0.18)	*0.34 (0.3,0.34)	*0.28 (0.23,0.33)	*0.63 (0.62,0.64)	*0.98 (0.94,1.02)
MA12	0.13 (0.12,0.15)	*0.31 (0.3,0.32)	0.26 (0.21,0.28)	*0.55 (0.54,0.56)	*0.92 (0.89,0.96)
MA44	0.15 (0.13,0.18)	*0.34 (0.3,0.36)	*0.28 (0.21,0.37)	*0.58 (0.57,0.59)	*0.82 (0.79,0.85)
MA53	*0.17 (0.15,0.21)	*0.32 (0.3,0.33)	*0.27 (0.21,0.33)	*0.60 (0.59,0.61)	*1.01 (0.96,1.05)
MA61	0.13 (0.12,0.16)	*0.35 (0.32,0.36)	*0.28 (0.23,0.35)	*0.67 (0.66,0.68)	*1.09 (1.05,1.12)
MA70	0.12 (0.1,0.14)	*0.30 (0.29,0.30)	0.21 (0.17,0.22)	*0.71 (0.7,0.73)	*1.02 (0.99,1.06)
MA71	*0.18 (0.15,0.22)	*0.30 (0.29,0.30)	0.21 (0.19,0.22)	*0.66 (0.65,0.67)	*1.33 (1.28,1.38)
NC2	0.12 (0.11,0.14)	0.29 (0.28,0.28)	0.20 (0.16,0.23)	*0.83 (0.82,0.84)	*1.2 (1.16,1.24)
NC30	0.13 (0.11,0.16)	*0.30 (0.30,0.30)	0.20 (0.19,0.20)	*0.68 (0.67,0.69)	*0.96 (0.93,0.99)
NC53	0.13 (0.11,0.15)	*0.31 (0.29,0.31)	0.25 (0.19,0.29)	*0.61 (0.6,0.62)	*1.12 (1.08,1.15)
NC9	0.15 (0.13,0.19)	*0.40 (0.33,0.47)	*0.38 (0.28,0.49)	*0.70 (0.7,0.72)	*0.58 (0.53,0.63)
NC94	*0.21 (0.19,0.24)	*0.45 (0.40,0.49)	*0.43 (0.34,0.49)	*1.02 (1.01,1.03)	*1.1 (1.04,1.15)

* Falls outside the confidence interval of Sam

[a] Measured as the ratio between the largest eigenvalue and the total variance.

[b] Difference in orientation based on Random Skewers.

Table 3: Disparity of shape and covariance based on their joint PCoA space (see Fig. 6). Covariance space is superimposed onto shape space for comparability. Calculations include all 24 PCoA dimensions that resulted in eigenvalues larger than zero. Numbers in parentheses indicate the equivalent calculations without strain 3045.

	Total	Mutants	Naturally-derived
Shape	0.042 (0.038)	0.021 (0.011)	0.029
Covariance	0.019 (0.019)	0.012 (0.011)	0.023

bioRxiv preprint doi: https://doi.org/10.1101/023333; this version posted July 27, 2015. The copyright holder for this preprint (which was not certified by peer review) is the author/funder, who has granted bioRxiv a license to display the preprint in perpetuity. It is made available under aCC-BY-NC 4.0 International license.

657

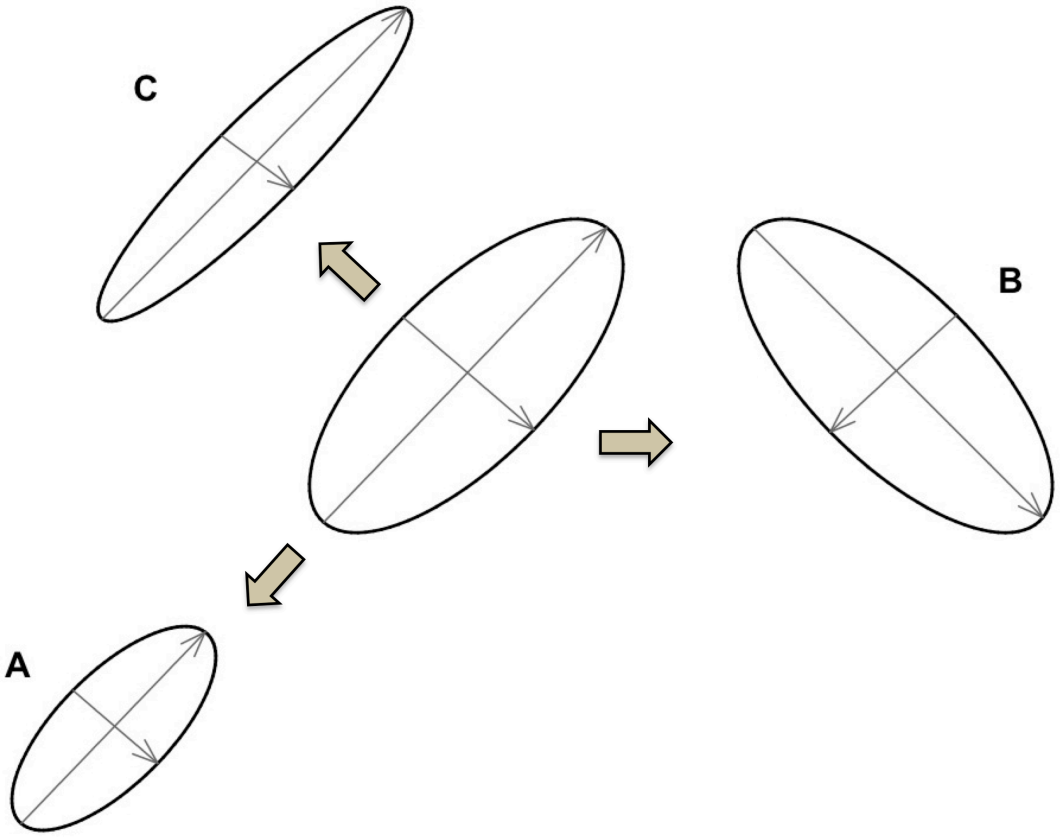

Figure1: Illustration of the different matrix properties. Ellipses represent 95% confidence interval of a normal bivariate distribution, and arrows (ellipse axes) represent orthogonal axes of covariaton. Matrices are presented as bivariate for illustration, but the principles are the same for multivariate. Ellipses A, B, and C represent a change in only one property each, relative to the ellipse in the middle. A, smaller matrix size (lower total variance); B, perpendicular orientation; C, higher eccentricity.

658

bioRxiv preprint doi: https://doi.org/10.1101/023333; this version posted July 27, 2015. The copyright holder for this preprint (which was not certified by peer review) is the author/funder, who has granted bioRxiv a license to display the preprint in perpetuity. It is made available under aCC-BY-NC 4.0 International license.

658
659

A

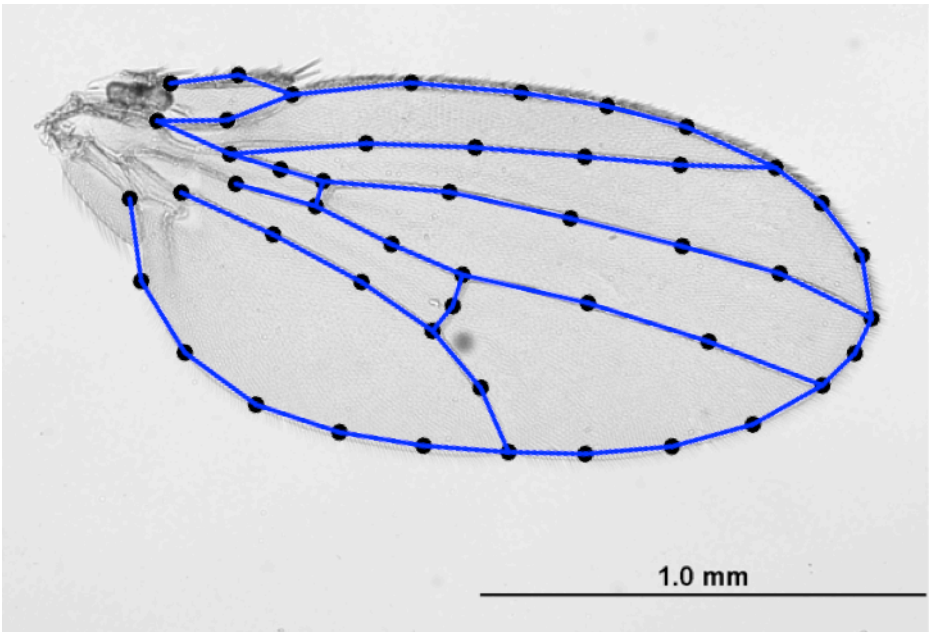

B

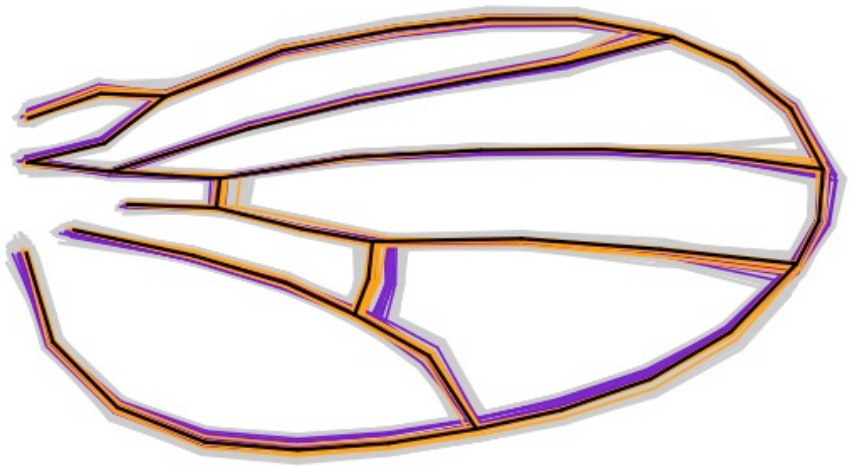

Figure 2: **A.** A representative wing image with fitted splines and the location of landmarks and semilandmarks along them. **B.** Individual variation in the sample (grey) relative to Sam (black), mutant means (orange), and means for naturally-derived lines (purple).

660
661

bioRxiv preprint doi: https://doi.org/10.1101/023333; this version posted July 27, 2015. The copyright holder for this preprint (which was not certified by peer review) is the author/funder, who has granted bioRxiv a license to display the preprint in perpetuity. It is made available under aCC-BY-NC 4.0 International license.

661
662

A

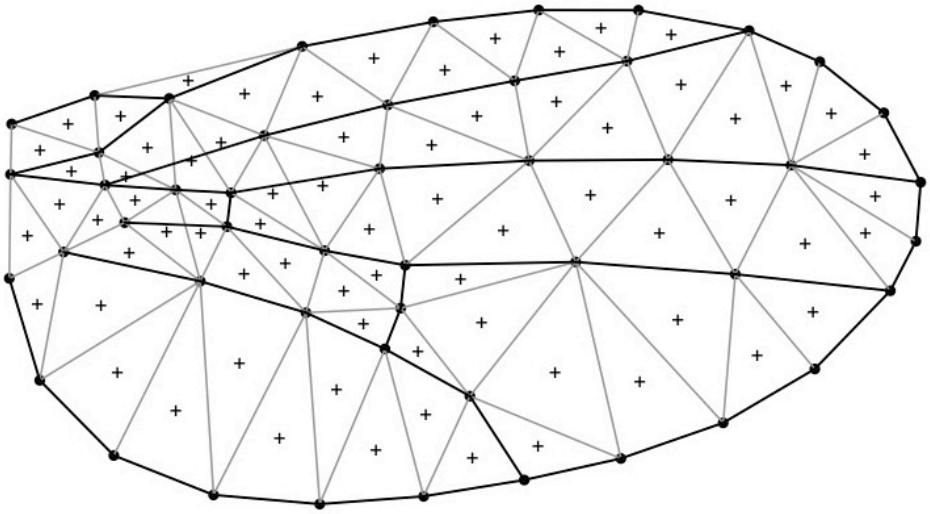

B

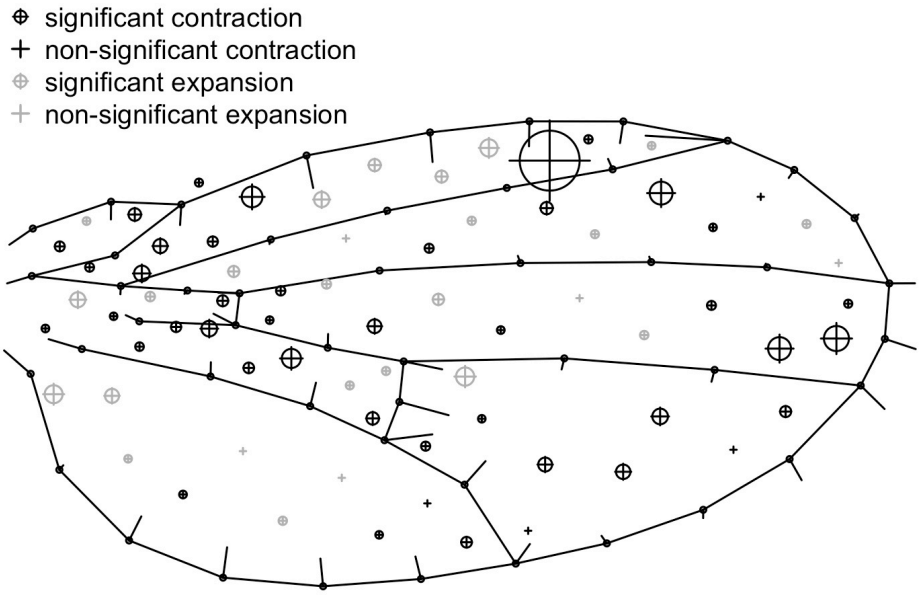

Figure 3: Illustrating the LORY method for interpolating shape changes from Procrustes data of genotype Bs^{k07909}. **A**, the tessellation scheme for choosing evaluation points. The landmarks and semi-landmarks (dots) are used as vertices. The centroids of the resulting triangles (crosses) are the final evaluation points. **B**, shape differences between the genotype mean and Sam inferred by calculating the Jacobians around each evaluation point, scaled by 100 (crosses and crossed circles). Bars represent the direction and change of differences between Sam and the sample mean at the landmarks and semi-landmarks based on the Procrustes data, scaled by 10X.

663

bioRxiv preprint doi: https://doi.org/10.1101/023333; this version posted July 27, 2015. The copyright holder for this preprint (which was not certified by peer review) is the author/funder, who has granted bioRxiv a license to display the preprint in perpetuity. It is made available under aCC-BY-NC 4.0 International license.

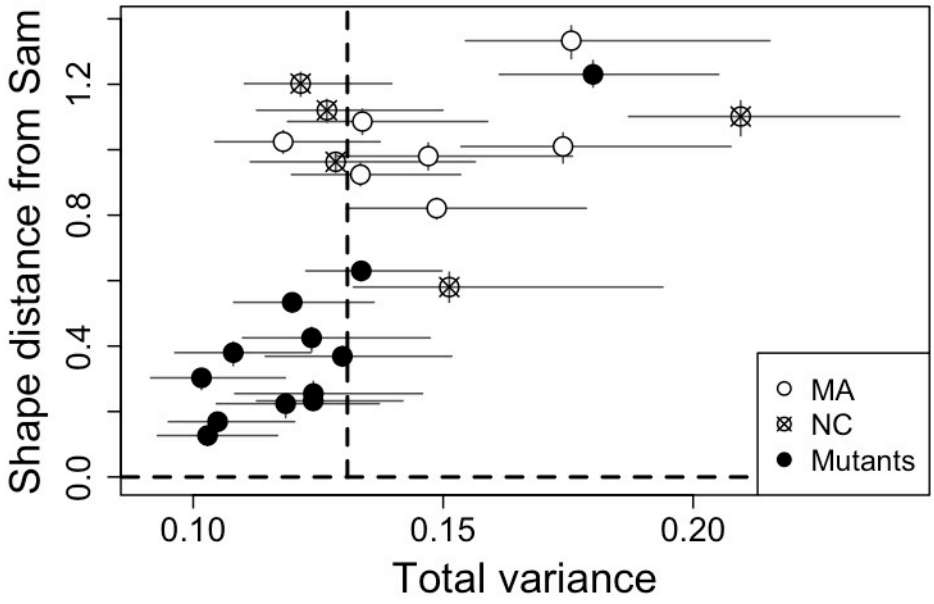

Figure 4: Mean-shape distance from Sam plotted against the total variance within each strain. Bars are 95% confidence intervals. Dashed lines represent values for the Sam wild type.

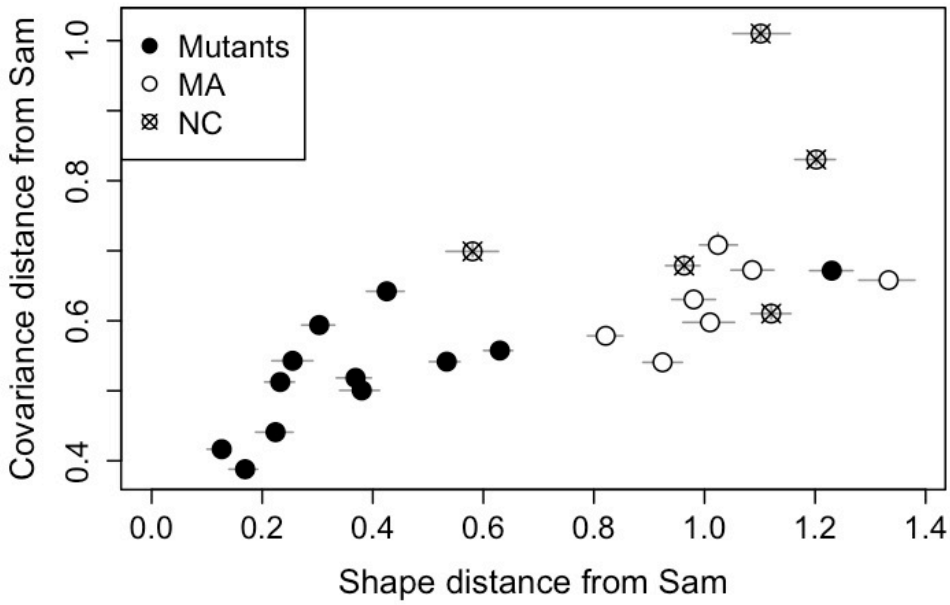

Figure 5: Covariance distance (i.e, difference in orientation), estimated by Random Skewers, plotted against mean-shape distance, relative to the Sam wild type. Bars are 95% confidence intervals.

bioRxiv preprint doi: https://doi.org/10.1101/023333; this version posted July 27, 2015. The copyright holder for this preprint (which was not certified by peer review) is the author/funder, who has granted bioRxiv a license to display the preprint in perpetuity. It is made available under aCC-BY-NC 4.0 International license.

667

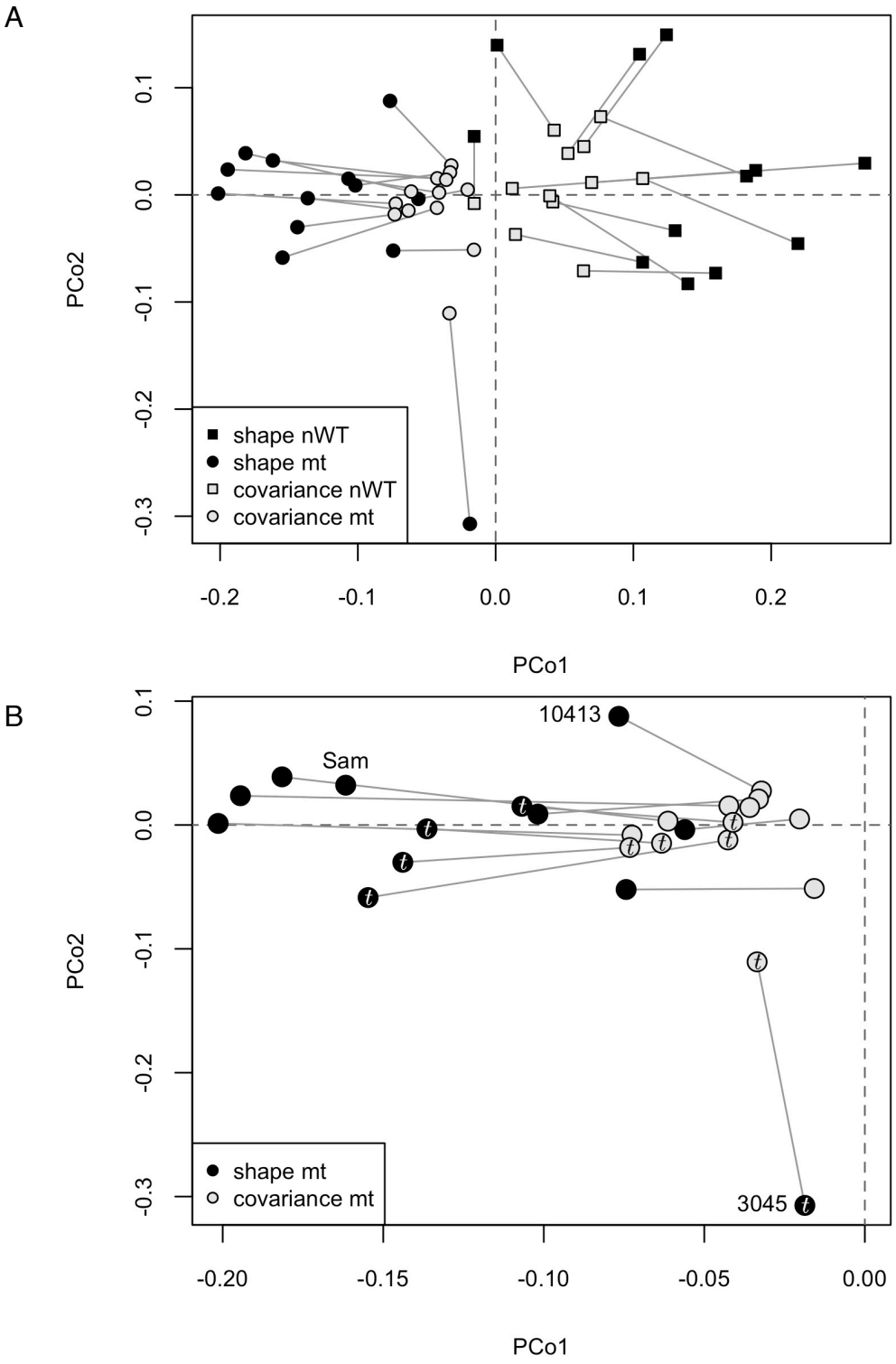

Figure 6: Covariance space superimposed onto shape space. Both spaces are based on all pairwise distances. Solid grey lines indicate the deviation between the two spaces for a given genotype. **A,** All genotypes; **B,** Mutants only, including the Sam wild type. Mutants that affect the TGF-β pathway are marked by *t*. All other mutants affect the EGFR pathway

bioRxiv preprint doi: https://doi.org/10.1101/023333; this version posted July 27, 2015. The copyright holder for this preprint (which was not certified by peer review) is the author/funder, who has granted bioRxiv a license to display the preprint in perpetuity. It is made available under aCC-BY-NC 4.0 International license.

668

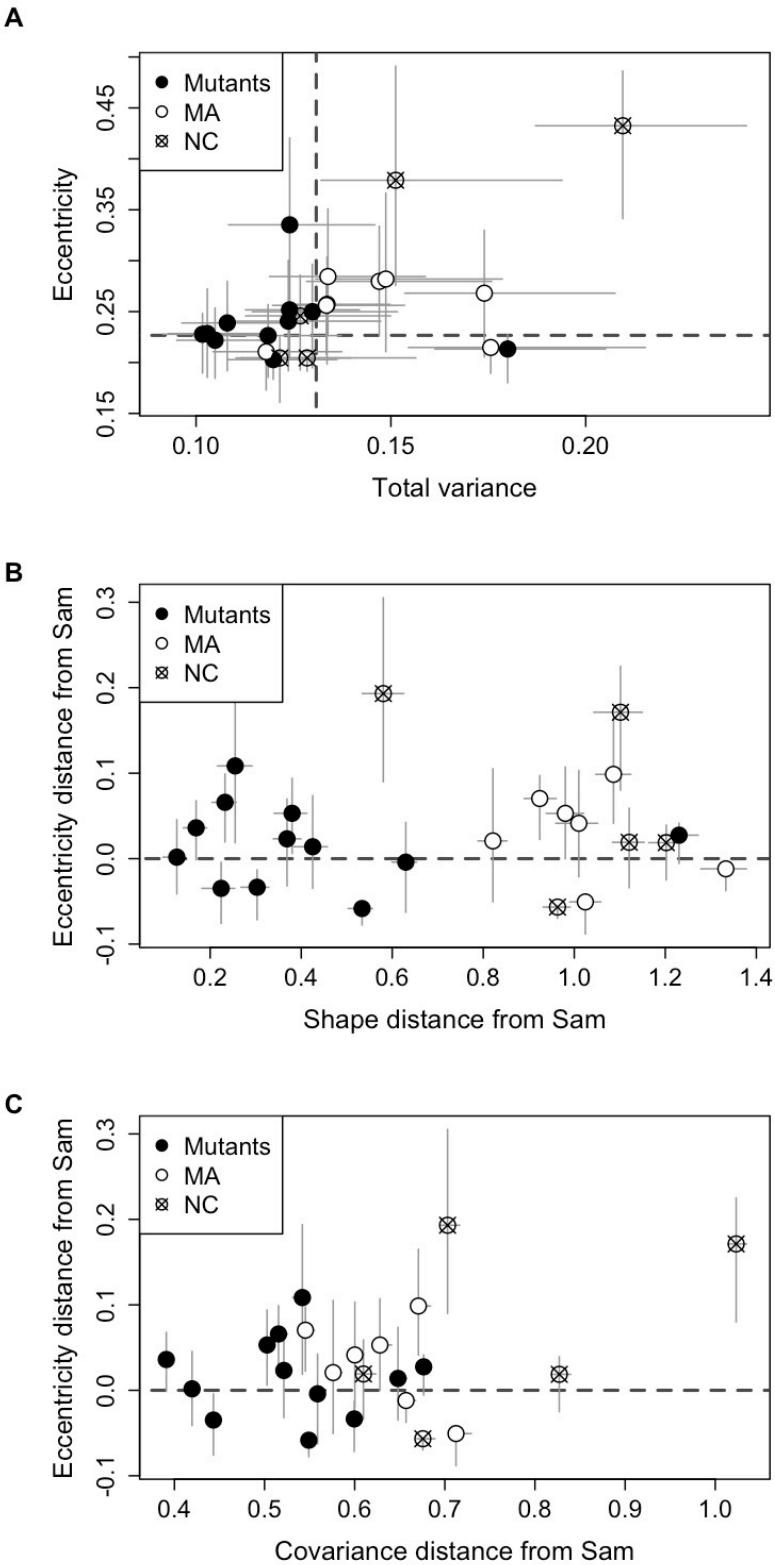

Figure 7: The association between eccentricity and total variance within each genotype (**A**), their mean-shape distance from Sam (**B**) and their covariance distance from Sam (**C**)

bioRxiv preprint doi: https://doi.org/10.1101/023333; this version posted July 27, 2015. The copyright holder for this preprint (which was not certified by peer review) is the author/funder, who has granted bioRxiv a license to display the preprint in perpetuity. It is made available under aCC-BY-NC 4.0 International license.

669